FACETS

FP6-2004-IST-FETPI 15879

Fast Analog Computing with Emergent Transient States

Deliverable D4-3

Report on the application of a two-variable model (e.g. the adaptive exponential integrate-and-fire model) with parameter sets for 4 prominent neuron types in the FACETS data base.

Report Version:	1.0
Classification:	Public
Type:	R
Due date:	2008.02.29.
Date issued:	2008.05.27.
Report Preparation:	Richard Naud, Wulfram Gerstner
Contract Start Date:	1 September 2005 Duration: 4 Years
Project Coordinator:	Karlheinz Meier (Heidelberg)
Partners:	ENSEIR Bordeaux, CNRS (Gif-sur-Yvette, Marseille), U Debrecen, TU Dresden, U Freiburg, TU Graz, U Heidelberg, EPFL Lausanne, Funetics S.a.r.l., U London, U Plymouth, INRIA, KTH Stockholm

Project funded by the European Community under the "Information Society Technologies" Programme

DELIVERABLE SUMMARY SHEET

Project Number: FP6-2004-IST-FETPI 15879

Project Acronym: FACETS

Title: Report on the application of a two-variable model (e.g. the adaptive exponential integrate-and-fire model) with parameter sets for 4 prominent neuron types in the FACETS database.

Deliverable N°: D4-3

Due date: 2008.02.29.

Delivery Date: 2008.05. 27.

Short description:

The adaptive exponential integrate-and-fire was fitted on experimental recordings done on cortical slices. In total, four types of cells were considered: excitatory regular spiking cells, inhibitory non-adapting, inhibitory continuously adapting, and low threshold spiking cells. For the latter the fit were done with the model from deliverable 4-2 as a reference. We describe the fitting methods and discuss how multiple firing patterns arise in the adaptive exponential integrate-and-fire. This report will be submitted to Biological Cybernetics as an original article. The deliverable comprises a manuscript for Biological Cybernetics augmented with the fitting of low threshold spiking cells.

Partners owning: LCN

Partners contributed: Report written by Richard Naud with help from Wulfram Gerstner (EPFL-LCN). Research done by EPFL-LCN (Richard Naud, Vincent Hirschi). Model of LTS cell used as a reference model in the annex from partner CNRS-Gif; the fit to the reference model in annex done by EPFL-LCN.

Made available to: FACETS members. Main part submitted to Biological Cybernetics.

Biological Cybernetics manuscript No.
(will be inserted by the editor)

Richard Naud · **Nicolas Marcille** · **Claudia Clopath** · **Wulfram Gerstner**

Versatility and Relevance of the Adaptive Exponential Integrate-and-Fire Model

Received: date / Revised: date

Abstract For simulations of large networks of spiking neurons, an accurate, simple and versatile single-neuron modeling framework is required. Here we explore the versatility of a simple two-equation model, the adaptive exponential integrate-and-fire. We show how this model can produce multiple firing patterns depending on the choice of parameter, and present a phase diagram describing the transition from one firing type to another. We give an analytical criterion to distinguish between continuous adaption, initial bursting, regular bursting and two types of tonic spiking. We report that the deterministic model is capable of producing irregular spiking when stimulated with constant current. Lastly, the simple model is fitted to real experiments of cortical neurons under step current stimulation. The results provide further support for the suitability of simple models such as the adaptive exponential integrate-and-fire for large network simulations.

1 Introduction

Large-scale simulations and theoretical investigations require neuron models that are mathematically tractable, biologically relevant and computationally fast. Moreover, a modeling framework should be versatile enough to span the whole diversity of neuron types by tuning a restricted number of parameters, avoiding the need of a new model for each class of neuron. Modeling the complete gating dynamics of ion channel densities in neuronal membranes satisfies only two of these five requirements: biological relevance and versatility. On the other hand, modeling a neuron either as a coincidence detector, as a resettable integrator or as firing poisson distributed spikes may fail to catch important aspects of single-neuron behavior. Small modifications to these simple models can bring them closer to reality. Lately multiple advances were made in that direction.

In the presence of high synaptic bombardment, modeling accurately the spike initiation is crucial and the Leaky Integrate-and-Fire (LIF) must be augmented by an exponential term to faithfully process fast inputs signals (Fourcaud-Trocme et al (2003)). An additional recovery variable is important to capture adaptation and resonance properties (Richardson et al (2003), Izhikevich (2003)). A simple quadratic model of spike initiation with a linearly dependent recovery variable and a reset in the state variables is sufficient to account for most types of firing patterns observed in the central nervous system (Izhikevich (2007)). Unlike a quadratic dependence on voltage, an exponential nonlinearity (Brette and Gerstner (2005)) keeps the subthreshold dynamics linear and matches direct measurments in cortical neurons (Badel et al (2007)). This last model - called the adaptive exponential integrate-and-fire (AdExp)[1] - was considered an accurate and convenient simplification to use in spiking network models. It is simple because it is described by only two equations and a reset condition. For the same reason it is computationally fast and could simulate even faster by transferring the solution methods developed for Izhikevich's model (Humphries and Gurney (2007)) to the AdExp. It is by construction closer to real neurons than the simplest of models, and it was shown to predict with high accuracy the spike timing of a conductance-based Hodgkin and Huxley model (Brette and Gerstner (2005)) and the spike timing of real pyramidal neurons under noisy current injection (Clopath et al (2007); Jolivet et al (2007)).

In this paper we address the versatility and the biological relevance of the aEIF model. We show how the aEIF reproduces multiple firing patterns and study the correspondence between the parameters and the firing types. Finally, we fit the model to experimental traces and obtain sets of parameters describing cortical fast spiking interneurons and regular spiking pyramidal neurons.

R. Naud
EPFL Station 15
Lausanne 1015
Switzerland
Tel.: +41-21-6936635
E-mail: richard.naud@epfl.ch

[1] Also referred to as aEIF.

2 Adaptive Exponential Integrate-and-Fire

The adaptive Exponential Integrate-and-Fire model (AdEx) describes the evolution of the membrane potential $V(t)$ when a current $I(t)$ is injected. It consists of a system of two differential equations:

$$C\frac{dV}{dt} = -g_L(V-E_L) + g_L\Delta_T \exp(\frac{V-V_T}{\Delta_T}) + I - w, \quad (1)$$

$$\tau_w\frac{dw}{dt} = a(V-E_L) - w, \quad (2)$$

and a reset condition that replaces the downswing of the action potential:

$$\text{if } V > 0\,\text{mV} \text{ then} V \rightarrow E_r \quad (3)$$

$$w \rightarrow w_r = w + b. \quad (4)$$

There are nine parameters required to define the evolution of the membrane potential (V) and the adapation current (w). The nine parameters can be separated into scaling parameters and bifurcation parameters. The scaling parameters are the parameters responsible for scaling the time axis, for the stretch and for the offset in state variables. The five scaling parameters are: total capacitance (C), total leak conductance (g_L), effective rest potential (E_L), threshold slope factor (Δ_T), effective threshold potential (V_T). Absorbing the parameters C andg_L to set the time scale $\tau_m = C/g_L$, Δ_T and V_T to set the membrane potential scale and offset, and appropriate rescaling of I and w, equation 1 can be reduced to a system of equation with dimensionless variables and only four parameters (Touboul (2008)). The remaining four parameters are bifurcation parameters (subthreshold adaptation, a, adaptation time constant, τ_w, spike triggered adaptation, b and reset potential V_r). Modifying these parameters brings qualitative changes in the behavior of the system.

The role of the bifurcation parameters is best understood through phase plane analysis (for an introduction see Izhikevich (2007)). Briefly, phase plane analysis involves plotting the state variables relative to each other. Nullclines represent the area in phase space in which a given variable remains constant. The V-nullcline (or w-nullcline) is defined as the set of points with $\frac{dV}{dt} = 0$ (or $\frac{dw}{dt}$ respectively). The shape and position of the nullclines depends on the parameters of the model. For instance changing the current in Eq. 1 involves an horizontal shift in the V-nullcline. The intersection of the two nullclines define fixed points which can be stable or unstable depending on the parameters of the model. In particular, the fixed points can loose or gain stability with changes in one or more parameters. As a bifurcation point, a change in the stability occurs, and this modifies the behavior of the system qualitatively. In the sytem of Eq. 1-2, the choice of subthreshold adaptation (a) and adaptation time constant (τ_w) determines wether an increase in current induces a loss of stability via an Andronov-Hopf or via a saddle-node bifurcation (Fig. 1). From a biological point of view, the bifurcation parameters, determine the strength of subthreshold oscillation, the presence of rebound spikes, and the firing pattern as we will see in the following section.

3 Multiple Firing Patterns

In order to study the range of firing patterns accessible with the AdExp, we simulate the injection of a step current. This is the most common experimental paradigm used by electrophysiologists to study and classify the classes of neurons (Markram et al (2004)). Mathematically, this situation corresponds the solution of Eq.'s 1-2 with constant current and initial values $V(0) = E_L$ and $w(0) = 0$. Similar to what is seen in real neurons, the response of the model is very diverse and depends on the model parameters. In Figure 3 we show an example of each firing pattern that can be produced by varying the parameters of the AdExp, the parameters associated with each example are given in Table 1. In this section we will describe how the different firing patterns arise in our simple model.

Sharp vs Broad Spike After Potential (SAP) The AdExp can produce adapting and tonic traces of two qualitatively different types. In Fig. 2a we see an example of the first type where the potential increases monotonically after a rapid downswing of the action potential. This type of reset is seen commonly in fast spiking interneurons, and it corresponds to a low value of the voltage reset V_r combined with weak spike-triggered adaptation b. In the phase plane we see that the reset is made to a point below the V-nullcline.

Broad SAP, on the other hand, are observed in regular spiking pyramidal neurons and in the continuously adapting interneurons. A broad SAP is recognized by its low curvature at all times after the spike (Fig. 2b). For a larger value of the spike-triggered adaptation parameter, the reset falls inside the V-nullcline, and this leads to the broad SAP. In this case the exact value of V_r is less relevant, since the membrane potential must decrease before being able to rise in preparation of the next spike.

The two types of SAP are modeled in the AdExp by two different spiking trajectories in the phase plane. These are determined by the location of the reset point in the phase plane. If the reset point is above the V-nullcline (recall that in that region $\frac{dV}{dt} < 0$ everywhere), the voltage will decrease before increasing in preparation of a spike, this trajectory is termed a broad SAP or broad reset. If the reset point is below the V-nullcline, the spiking trajectory starts to increase immediately after the reset ($\frac{dV}{dt} < 0$ everywhere below the V-nullcline), and the SAP appears as a sharp reset. We can write this distiction as an analytical relation that depends on the reset point (E_r, w_r). There is a broad reset if

$$w_r > -g_L(E_r - E_L) + g_L\Delta_T \exp\left(\frac{E_r - V_T}{\Delta_T}\right) + I, \quad (5)$$

and otherwise the reset is sharp.

Tonic vs Adapting The simplest type of spiking pattern is the regular discharge of action potentials (tonic firing, see Fig. 3a). This firing pattern is the only firing pattern that a standard leaky or non-leaky integrate-and-fire model can generate. In the framework of the AdExp, it corresponds to the absence of spike-triggered adaptation and subthreshold adaptation ($a, b = 0$). Most neurons, however, show some level of spike-frequency adaptation. In this firing pattern, the inter-spike interval (ISI) grows during a sustained stimulus (Fig. 3b). The classification between adapting and non adapting can be drawn from the adaptation index:

$$A = \frac{1}{N-k-1}\sum_{i=k}^{N}\frac{isi_i - isi_{i-1}}{isi_i + isi_{i-1}} \tag{6}$$

where $k \geq 2$ is used to disregard any initial transient. Consistent with other studies (Druckmann et al (2007)) we take $k = 4$, i. e. we disregard the first two inter-spike intervals . Typically fast spiking interneurons have an adaptation index of 0.005 whereas regular spiking pyramidal neurons have A = 0.015 (with N = 15 to 40 spikes, Druckmann et al (2007)). Since the adaptation stabilize after a certain number of spikes, computing the adaptation index will depend on the number of spikes considered. In this article, we will compute the adaptation index with N fixed to 20 spikes.

Initial Bursting Initial bursting denotes a group of spikes that were emitted at a frequency considerably greater than the steady-state frequency. This definition is very ambiguous and in many experimental traces initial bursting is indistinguishable from pronounced adaptation. In the framework of the AdExp, a clear definition becomes apparent. Initial bursting arises when the spiking starts with at least one sharp reset followed by broad resets only (Fig. 3c).

Regular Bursting Regular bursting appears in a scenario similar to initial bursting except that the first broad reset projects below at least one of the previous reset points in the phase plane, such that the next reset point is below the V-nullcline, i. e. the next reset is sharp (Fig. 3d). This situation leads to an alternation between sharp and broad resets. Regular bursting is made possible with a V_r higher than the threshold so as to shield some reset points on the right hand side of the V-nullcline.

Delayed Spiking and Facilitation A negative a acts as a subthreshold facilitation which can be responsible for delayed initiation. Delayed spiking appears when injecting a current close to the rheobase. The adaptation current is slowly decreasing at a depolarized V, allowing the neuron to spike once the adaptation has decreased sufficiently (Fig. 3e). In the phase plane, the trajectory of the first spike must contour the V-nullcline, this is slow because the magnitude of $\frac{dV}{dt}$ decreases in approach of the V-nullcline. This system can lead to facilitation if the spike-triggered adaptation b is weak, as shown in Fig. 3e. For greater values of spike-triggered adaptation, it is also possible to get a delayed adapting trace (not shown) and a delayed bursting trace (Fig. 3f).

Rebound or Transient Spikes Post-inhibitory rebound is seen in several types of neurons. When a hyperpolarizing step current is released abruptly, some neurons will spike one or several time(s) before reaching their state of rest. This phenomenon is very similar to transient spiking observed during a step of depolarizing current. In both cases the sudden increase in current does not induce a loss of stability. A spike is nevertheless produced because the adaptation current is too slow to compensate the sharp change in current. If the applied current were modified gradually across the same absolute change that produces transient spiking, the neuron would not spike because it would have had time to adapt. In the phase plane, rebound corresponds to a situation where the initial condition is situated outside the separatrix that delimits the area of trajectories converging to the stable fixed point (Fig 3g).

Irregular Spiking Irregular spiking can occur in an AdExp model despite the fact that the equations are deterministic. Irregular spiking is manifest when the interspike interval keep on changing seemingly without periodicity. As for the regular bursting firing pattern, there is an alternation of sharp and broad resets, but the sequence is not periodic. This behavior appears for a restricted set of parameters, and the volume occupied by the irregular spiking pattern in the parameter space seems very small. We verified that the behavior was not due to a numerical artifact by reducing the integration time step. The irregular pattern was conserved if we reduced the timestep from 10 μs to 1 μs. Though other region of the parameter space may produce irregular spiking, we found a region that corresponds to negative subthreshold adaptation, large spike-triggered adaptation and high voltage reset (Fig. 3h).

For a given set of parameters, irregular spiking is manifest on a narrow range of injection current Fig. 4a. We check that this set of parameter was associated with chaos Strogatz (1994) by testing the dependence of the numerical integration on the initial conditions. We perturbed the initial conditions by a very small value $\delta = 10^{-12}$ and evaluate the error in the adaptation variable at each spike:

$$E = (w(\hat{t}_i) - w_\delta(\hat{t}_i))^2 \tag{7}$$

where $w(\hat{t}_i)$ and $w_\delta(\hat{t}_i)$ is the adaptation current at spike i for the unperturbed and perturbed initial condition, respectively. Fig. 4b shows that this error grows exponentially with the number of spike. The slope of the semi-log plot is 2.56. Similar to the Lorenz map, we can plot the magnitude of the interspike interval with respect to the preceding interpike interval. After a very large number of spikes (n = 1240), this function appears as a continous function (Fig. 4c).

4 Parameter Space

Given the definitions for each firing pattern, we can now investigate how these firing patterns depend on the specific set of parameters. Since this problem depends heavily on the

bifurcation parameters, we fixed the scaling parameters to realistic values : $C = 100$ pF, $g_L = 10$ nS, $E_L = -70$ mV, $V_T = -50$ mV and $\Delta_T = 2$ mV. Changing the scaling parameters will not change the set of firing patterns accessible for a given set of bifurcation parameters but may modify the amount of current necessary to go from one firing type to another. In addition, some firing patterns exist only close to the rheobase current (delayed spiking, transient spiking). In this section we will consider only the firing patterns that appear at step current twice greater the rheobase current. This rheobase was determined according to analytical expressions given in Touboul (2008) and corresponds to the ramp current at which the neuron begins to spike. The firing pattern is likely to change for different step current amplitudes, but characterizing parameter sets according to the accessible sequence of firing patterns goes beyond the scope of the present study.

For each set of the bifurcation parameters, Eq.'s 1-4 were solved with the exponential Euler numerical solution method with a time step of 0.005ms, we stopped the simulation after 50 spikes or 1000 seconds, and characterized the firing pattern according to the following simple rules:

- Tonic: Strictly sharp resets or strictly broad resets and $A < 0.01$.
- Adapting: Strictly sharp resets or strictly broad resets and $A > 0.01$.
- Initial bursting: Ordered sequence of each type of resets (e. g. sharp - sharp - broad - broad - broad).
- Regular bursting: Alternation between broad and sharp SAP such that the number of sharp resets between each broad reset is constant.
- Irregular spiking: Alternation between broad and sharp SAP such that the number of sharp resets between each broad reset is not constant.

The range of bifurcation parameters considered was limited to realistic values for spiking neurons ($V_r \in [-70, -40]$ mV, and $b \in [0, 500]$ pA). All programs were written in Matlab (The Mathworks, Natick, MA) and ran on a personal computer.

In Fig. 5, the distribution of firing patterns is shown as a function of the reset parameters V_r and b with fixed values of a and τ_w. The fixed τ_w was 5 ms or 100 ms such that the w-variable can be interpreted as a refractory current or an adaptation current, respectively. The a parameter was fixed to 0.001 nS or 30 nS corresponding to a system loosing stability via a saddle-node or Andronov-Hopf bifurcation, respectively.

The adaptive models have bursting firing patterns extending to larger areas in the parameter space than the refractory models, which have their diversity almost uniquely constrained to resets higher than the threshold. In all cases, the shape of an exponential is recognized and forms the border between bursting (initial or regular) and tonic-adapting firing patterns. In Fig. 5a and 5b, the tonic spiking at low b and at high b corresponds to tonic with sharp resets and tonic with broad resets, respectively. On the other hand, an adaptive current with high subthreshold adaptation yields predominantly bursting (initial and regular) and adapting firing patterns. A strong subthreshold adaptation is not sufficient on its own, however, to model adapting and bursting pattern as we see in Fig. 5d, but needs to be combined with large values of V_r. The refractory time constant in that case is often smaller than the interspike interval, this prevents cumulative increase of w since the adaptation current decays almost completely between spikes.

Delayed spiking, transient spiking are absent from Figure 5 because these firing patterns do not exist when the current is well above the rheobase. Delayed spiking will appear at injection current slightly above the rheobase and are more salient at low or negative a. Transient spiking is produced with current not sufficient to make the stable fixed point loose stability, and this firing pattern depends heavily on a as it is can occur only for sizable a. Irregular spiking could be part of Fig. 5, but the region may be too small to be seen on the scale of the graph.

5 Comparison with Cortical Neurons

We can test that the AdExp accurately reproduces the firing patterns of real neurons by comparing with experimental injections of step currents into neurons of the cortex (data, courtesy of Henry Markram, Maria Toledo-Rodriguez and Felix Schürmann, see Markram *et al.* (2004) and Toledo-Rodriguez *et al.* (2004) for the complete details on the experiments). Briefly, the experiments consist of 2-5 repetitions of 2 seconds step current injections with three different amplitudes. The amplitude of the steps ranged from 100 to 200 pA. The electrophysiological class was defined by Markram et al. (2004) for the inhibitory neurons and according to Connors and Gutnick (1990) . We will be considereing only three different classes. In particular we will comapre the AdExp with two types of inhibitory neurons (continuous accomodating, cAD, and continuousn non-adapting, cNA) and one type of excitatory neuron (regular spiking, RS).

In order to compare the experiments with the parameter set that represents each neuron the best, we fit the parameters neuron per neuron. The fitting method was chosen for the ease of implementation and for the capability to handle an optimization problem with many local minima. The detailed description is postponed to the end of this Section. Optimized model traces are compared with the experimental traces in Fig. 6. We can see that the AdExp offers a good qualitative match akin to optimized HH models (Druckmann et al (2007)). The optimized parameters for each chosen cell are given in Table 1. From this table, we see that the inhibitory cells correspond to smaller membrane capacitance, consistent with the smaller size of these cells. The subthreshold adaptation is low for all three cells and does not influence strongly the features used as optimization criteria, but other cell types are believed to have high a such as low threshold spiking (LTS) interneurons neurons. The timescale of the adaptation is the largest for the RS cells, which is expected

due to slow adaptation currents known to be present in these cells.

Optimization Methods We used data that was collected before the protocol to determine the parameters suggested by Brette and Gerstner (2005) was published. Here we will describe the optimization methods used to find the best set of parameters ($\boldsymbol{\beta}$). Inspired from Druckmann et al (2007) and Vanier and Bower (1999), we used a MATLAB implementation of a genetic algorithm (The Mathworks, Natick, MA) to solve the optimization problem. The cost associated with a parameter set, $C(\boldsymbol{\beta})$, was defined with eight features of the observed responses. The eight features are:

- f_1: Number of spikes, n,
- f_2: First spike latency,
- f_3: First inter-spike interval,
- f_4: Second inter-spike interval,
- f_5: Last inter-spike interval,
- f_6: First inter-spike minimum potential,
- f_7: Second inter-spike minimum potential,
- f_8: Waveform before the first spike.

The spike times were defined as zero-crossings and the inter-spike minimum potential was taken to be the lowest voltage observed between the first and the second spike. For each feature we define a $\overline{\chi}^2$ which averages the χ^2 value across all three step current amplitudes. Illustrating this with the first feature we have:

$$\overline{\chi}_1^2 = \frac{1}{3}\sum_{j=1}^{3} \frac{\langle n_j^{(obs)} \rangle - n_j^{(\boldsymbol{\beta})}}{Var[n_j^{(obs)}]} \tag{8}$$

where n_j is the number of spikes for stimulus amplitude j observed in experimental traces (obs) or in a model with parameters $\boldsymbol{\beta}$. The angular brackets denote the average and *Var* the variance of the observed features across the repetitions. A similar equation can be written for each feature except for feature 8:

$$\overline{\chi}_8^2 = \frac{1}{3}\sum_{j=1}^{3} \frac{\int \left(V^{(obs)}(t) - V^{(\boldsymbol{\beta})}(t)\right)^2 dt}{(0.1mV)^2} \tag{9}$$

where the integral runs from the onset of the step to two standard deviation before the mean first spike latency. Then the cost associated with a parameter set is:

$$Cost = \sum_{i=1}^{8} \overline{\chi}_i^2. \tag{10}$$

This is minimized with a genetic algorithm with a population of 100 individuals for 500 generations.

6 Discussion

We have seen that the AdExp model can produce multiple firing patterns depending on parameters. The model neuron can be initially bursting, regularly bursting, tonically spiking, adapting, facilitating, irregular spiking or show delayed initiation, and this depends mainly on four parameter values. We have drawn clear definitions of these firing patterns in terms of two types of spiking trajectories. The two types of spiking trajectories depends on wether the adaptation current immediately after spiking is strong enough to make the membrane potential decrease slowly before starting to increase in preparation for the next spike. These analytical definitions, and especially an explicit distinction between continuous adaptation and initial bursting, make useful expansion of the previous work on simple models (Izhikevich (2003, 2007); Touboul (2008)). Furthermore, irregular spiking with an AdExp model has not been reported before.

We have seen that this simple neuron model can be fit with good agreement to three types of cortical neurons, as can be seen from the comparison between model and experimental traces on the time scale of seconds (two first columns in Fig. 6). A closer look on the overlay unveils some discrepancies: the spike initiation of the cAD interneurons is not fully captured by the model, the first interspike interval is too long in the case for the RS cell while the last interspike interval is too short in the cNA cell. This makes the tradeoff between different features evident, and our simple model cannot fit with high precision both the initial burst of RS cells and the broad SAP observed in these cells. Important improvement is to be expected by adding another adaptation current but here we restricted the investigation to the capability of only one adaptation variable. These results must be seen in the context of previous studies which showed the high predictive power of the AdExp when modeling spike timing of noisy current injection (Brette and Gerstner (2005); Jolivet et al (2007)).

Throughout this article, the biological justification for the adaptation current was not precisely determined. This adaptation current can be purely due to ion channels such as I_M and $I_K^{(slow)}$ (Destexhe et al (1998); Korngreen and Sakmann (2000)), or by a slowly charging passive dendritic compartment. Considering the latter alternative, we can put our results in contrast with the work of Mainen and Sejnowski (1996), where it was shown that variable electrical coupling with an active dendritic compartment can be made responsible for multiple firing patterns. In the AdExp, one can interpret a high voltage reset as an action potential with an after-spike depolarization which itself depends on the coupling with a dendritic compartment. Yet the AdExp framework is consideribly simpler than the Pinsky-Rinzel or Hodgkin-Huxley models used by Mainen and Sejnowski.

We can conlude that the diversity of firing patterns is explained by simple underlying dynamical processes. The AdExp model represents an attractive alternative to use in large-scale network simulations. Earlier studies have shown that it is sufficiently accurate for the prediction of spike tim-

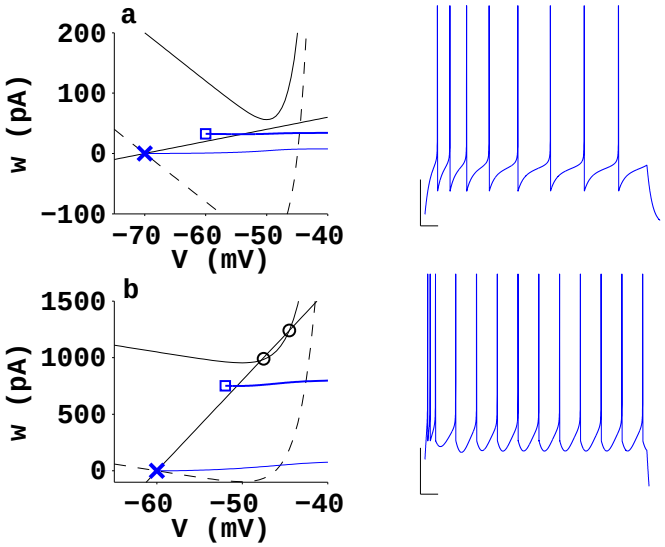

Fig. 1 Phase plane portrait of a step current injected in a aEIF model where a saddle-node bifucation is responsible for the loss of stability (a), and where the Andronov-Hopf bifurcation is responsible for the loss of stability (b). In the phase planes the trajectories of the first and second spikes are shown in blue. The resting state is indicated by the large blue cross. The nullclines are shown in black: the w-nullcline is the straight line (green), the V-nullcline in the absence of current is the curved dash line, the V-nullcline in the presence of stimulating current is the curved solid line (black). Unstable fixed points are encircled. The scale bars corresponds to 20 mV vertically and 20 ms horizontally. The maximal current injected was 230 pA for the saddle-node bifurcation, and 550 pA for the Andronov-Hopf bifurcation. As the current increases, the V-nullcline shifts upwards. This makes the two fixed points move toward each other. In the saddle-node bifurcation, the fixed points dissappear after the stable fixed point merges with the unstable fixed point. In the Andronov-Hopf bifurcation, the stable fixed point looses stability before the V-nullcline leaves the w-nullcline.

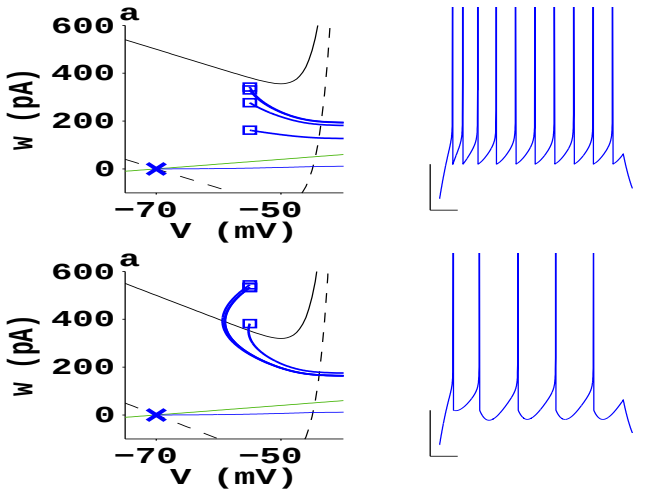

Fig. 2 Phase portrait and associated traces illustrating two types of tonic spiking: tonic spiking with sharp reset (a) and tonic spiking with broad reset (b). In both cases we see some degree of adaptation, yet both traces do not belong to the continuously adapting class described in the text because there is no substantial adaptation beyound the first two inter-spike interval.

ing when a regular spiking pyramidal neuron receives noisy current injection at the soma (Jolivet et al (2007)). Large network simulations such as simulations of a cortical column (Markram (2006)) or even larger systems (Hill and Tononi (2005); Izhikevich and Edelman (2008)) require a different model for each neuron type. In this paper we addressed this issue by providing parameter sets that describe three types of cortical neurons. Further work will be needed to extend this to a larger number of neuron types and stimulation paradigms.

Acknowledgements Many thanks to Henry Markram, Felix Schürmann and Maria Toledo-Rodriguez for providing the experimental traces. R. Naud is supported by the *Fonds Québécois de la Recherche sur la Nature et les Technologie* (FQRNT). This project is partly supported by funding of the European Union under the grant no. 15879 (FACETS)

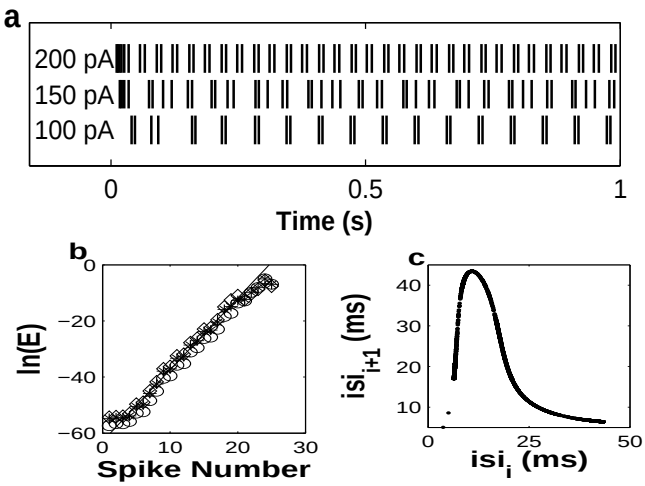

Fig. 4 Irregular firing is a manifestation of chaos in the AdExp. Spikes times of an irregular spiking model are shown in **a** for three different amplitudes of the stimulating current step. The middle current amplitude ($I = 150pA$) spikes without periodicity, this current amplitude was used to make **b** and **c**. In **b** we show that numerical integration of an irregular spiking model depends heavily on the initial conditions, such that $ln(E)$ grows exponentially with the number of spikes simulated. The stars denote an modification of the initial condition in w only, the diamonds is a modification in V and the circles a modification in w and w. A linear fit shows a slope of 2.56 (full line). In **c** we plot each interspike interval in function of the precedent ISI (n = 1240 spikes). The parameters for the irregular spiking model are given in Table 1.

References

Badel L, Lefort S, Brette R, Petersen C, Gerstner W, Richardson M (2007) Dynamic i-v curves are reliable predictors of naturalistic pyramidal-neuron voltage traces. J Neurophysiol DOI 10.1152/jn.01107.2007

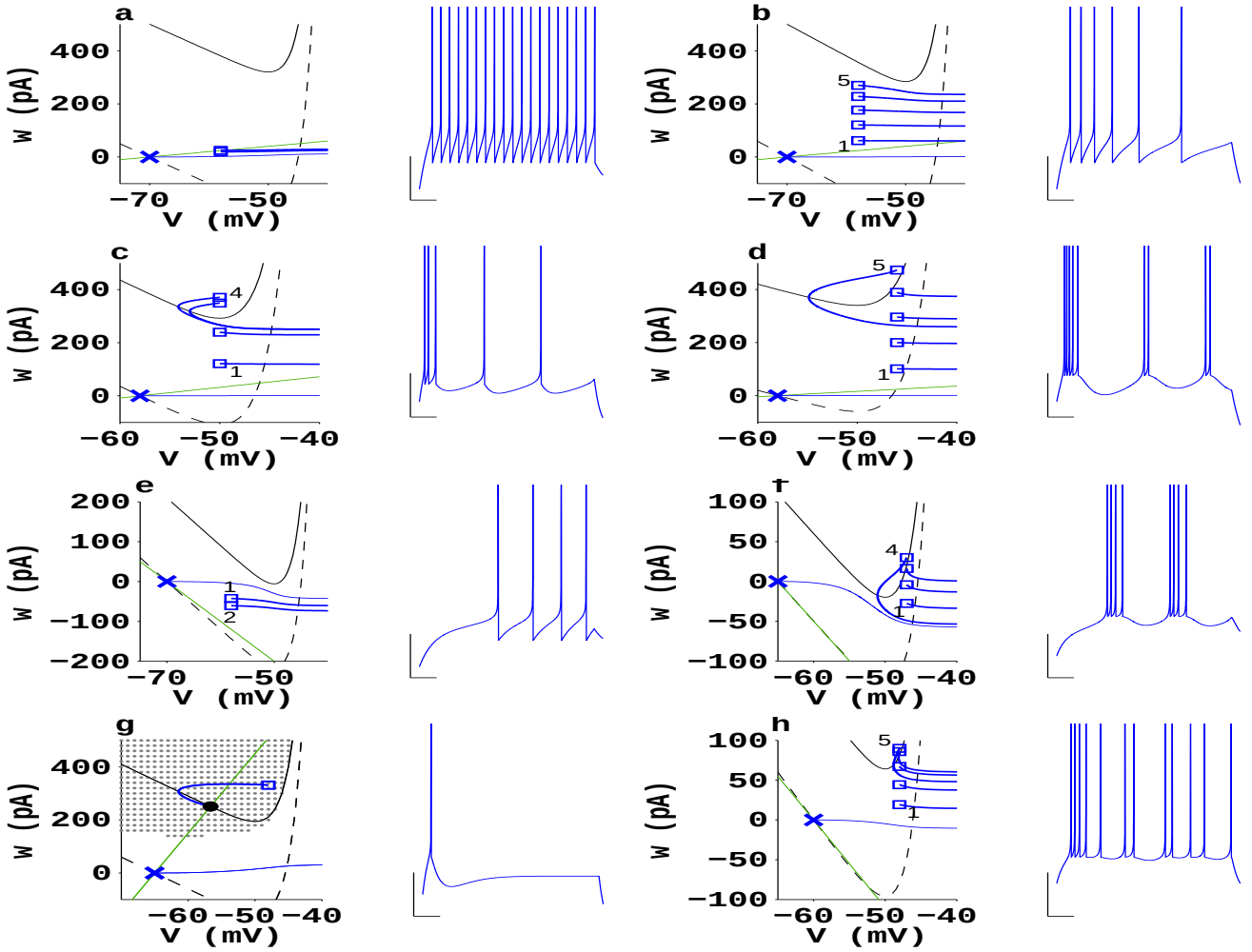

Fig. 3 Phase plane description of four firing patterns. Firing patterns observed during a step current stimulation are: tonic spiking (a), adaptation (b), initial burst (c), regular bursting (d), delayed facilitating (e), delayed regular bursting (f), transient spiking (g) and irregular spiking (h). The voltage traces are shown with a scale bar that corresponds to 100 ms and 20 mV. The traces are plotted in their corresponding phase planes as a trajectory in the two state variables (full blue line). The nullclines are shown in black, the w-nullcline is a straight line, the V-nullcline before current stimulation is the curved dash line, and in the presence of stimulation it is the curved solid line. The stable fixed points are in marked with a black circle, the state of rest by a blue cross and the first 1-5 resets by blue squares. Comparing b with c illustrates that reset points that jump above the V-nullcline lead to initial bursting. Comparing c with d illustrates that regular bursting is obtained when the first broad reset maps below at least one of the previous rest points.

Brette R, Gerstner W (2005) Adaptive exponential integrate-and-fire model as an effective description of neuronal activity. J Neurophysiol 94(5):3637–3642, DOI 10.1152/jn.00686.2005

Clopath C, Jolivet R, Rauch A, Luscher HR, Gerstner W (2007) Predicting neuronal activity with simple models of the threshold type: Adaptive exponential integrate-and-fire model with two compartments. Neurocomputing 70(10-12):1668–1673

Connors BW, Gutnick MJ (1990) Intrinsic firing patterns of diverse neocortical neurons. Trends Neurosci 13(3):99–104

Destexhe A, Contreras D, Steriade M (1998) Mechanisms underlying the synchronizing action of corticothalamic feedback through inhibition of thalamic relay cells. J Neurophysiol 79(2):999–1016

Druckmann S, Bannitt Y, Gidon AA, Schuermann F, Segev I (2007) A novel multiple objective optimization framework for constraining conductance-based neuron models by experimental data. Front Neurosci 1(1)

Fourcaud-Trocme N, Hansel D, van Vreeswijk C, Brunel N (2003) How spike generation mechanisms determine the neuronal response to fluctuating inputs. J Neurosci 23(37):11,628–11,640

Hill S, Tononi G (2005) Modeling sleep and wakefulness in the thalamocortical system. J Neurophysiol 93(3):1671–1698, DOI 10.1152/jn.00915.2004

Humphries MD, Gurney K (2007) Solution methods for a new class of simple model neurons. Neural Comput 19(12):3216–3225, DOI 10.1162/neco.2007.19.12.3216

Izhikevich EM (2003) Simple model of spiking neurons. IEEE Trans Neural Netw 14(6):1569–1572, DOI 10.1109/TNN.2003.820440

Izhikevich EM (2007) Dynamical systems in neuroscience : the geometry of excitability and bursting. MIT Press, Cambridge, Mass.

Izhikevich EM, Edelman GM (2008) Large-scale model of mammalian thalamocortical systems. Proc Natl Acad Sci U S A 105(9):3593–3598, DOI 10.1073/pnas.0712231105

Jolivet R, Kobayashi R, Rauch A, Naud R, Shinomoto S, Gerstner W (2007) A benchmark test for a quantitative assessment of simple neuron models. J Neurosci Methods DOI 10.1016/j.jneumeth.2007.11.006

Table 1 Parameters and cost for fits shown in Fig. 6 and for firing pattern example shown in Fig. 3.

Type	C (pF)	g_L (nS)	E_L (mV)	V_T (mV)	Δ_T (mV)	a (nS)	τ_w (ms)	b (pA)	V_r (mV)	$C(\boldsymbol{\beta})$	I (pA)
cNA	54	4.5	-61.3	-42.2	3.0	0	22	59	-54.4	15.1	184
cAD	76	4.2	-62.7	-54.7	7.1	0.54	46.6	45.6	-54.7	23.9	116
RS	103	4.4	-65.6	-53.6	1.5	-0.74	90.2	64	-53.7	19.6	98
Fig. 3a	200	10	-70	-50	2	2	30	0	-58	-	500
Fig. 3b	200	12	-70	-50	2	2	300	60	-58	-	500
Fig. 3c	130	18	-58	-50	2	4	150	120	-50	-	400
Fig. 3d	200	10	-58	-50	2	2	120	100	-46	-	210
Fig. 3e	200	12	-70	-50	2	-10	300	0	-58	-	300
Fig. 3f	200	12	-70	-50	2	-6	300	0	-58	-	110
Fig. 3g	100	10	-65	-50	2	-10	90	30	-47	-	350
Fig. 3h	100	12	-60	-50	2	-11	130	30	-48	-	160

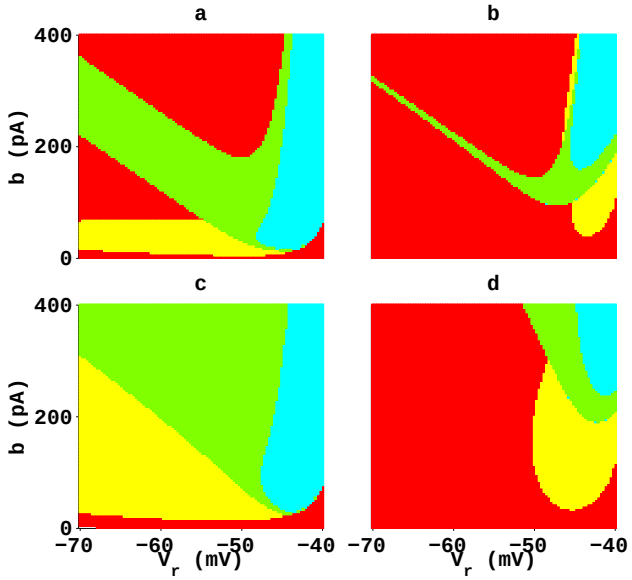

Fig. 5 Parameter space exploration of the four bifurcation parameters. Tonic spiking in red, adapting in yellow, initial bursting in green and regular bursting in cyan. The four-dimensional parameter space was reduced to four relevant planes: **a** Adaptive time constant (τ_w = 100 ms) and saddle-node bifurcation (a = 0.001 nS), **b** refractory time constant (τ_w = 5 ms) and saddle-node bifurcation (a = 0.001 nS), **c** Adaptive time constant (τ_w = 100 ms) and Andronov-Hopf bifurcation (a = 30 nS), **d** refractory time constant (τ_w = 5 ms) and Andronov-Hopf bifurcation (a = 30 nS). The firing pattern was classified for infection of current twice the rheobase, according to the criteria exposed in Sect. 3.

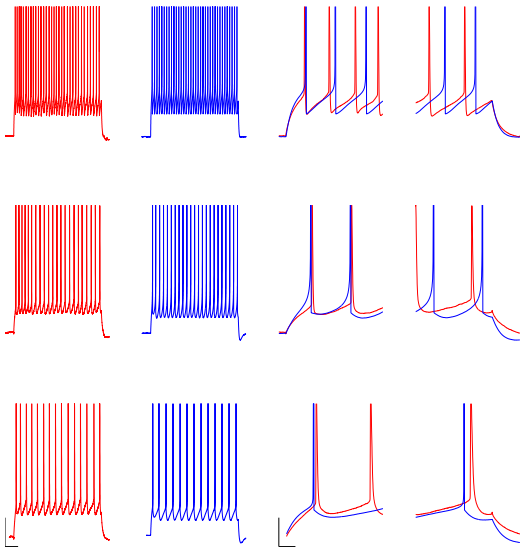

Fig. 6 Comparison of the aEIF with three types of cortical neurons on step current injections. From left to right: experimental traces (red), aEIF model (blue), and overlay of the traces during onset and offset of the current step. From top to bottom: cNA, cAD, and RS. The left scale bar shows 20 mV and 300 ms, the scale bar for the overlays shows 20 mV and 20 ms. The current injections corresponds to 150 pA for cNA, 105 pA for cAD, and 130 pA for RS. Only one of the 5 repetitions are shown for clarity. Across multiple repetition of the same stimulus, the time of the first spike or the firsts interspike intervals may jitter around what is seen on this figure.

Korngreen A, Sakmann B (2000) Voltage-gated k+ channels in layer 5 neocortical pyramidal neurones from young rats: subtypes and gradients. J Physiol 525 Pt 3:621–639

Mainen ZF, Sejnowski TJ (1996) Influence of dendritic structure on firing pattern in model neocortical neurons. Nature 382(6589):363–366, DOI 10.1038/382363a0

Markram H (2006) The blue brain project. Nat Rev Neurosci 7(2):153–160, DOI 10.1038/nrn1848

Markram H, Toledo-Rodriguez M, Wang Y, Gupta A, Silberberg G, Wu C (2004) Interneurons of the neocortical inhibitory system. Nat Rev Neurosci 5(10):793–807, DOI 10.1038/nrn1519

Richardson MJE, Brunel N, Hakim V (2003) From subthreshold to firing-rate resonance. J Neurophysiol 89(5):2538–2554, DOI 10.1152/jn.00955.2002

Strogatz SH (1994) Nonlinear dynamics and Chaos: with applications to physics, biology, chemistry, and engineering. Addison-Wesley Pub., Reading, Mass., URL http://www.loc.gov/catdir/enhancements/fy0830/93006166-d.html

Toledo-Rodriguez M, Blumenfeld B, Wu C, Luo J, Attali B, Goodman P, Markram H (2004) Correlation maps allow neuronal electrical properties to be predicted from single-cell gene expression profiles in rat neocortex. Cereb Cortex 14(12):1310–1327, DOI 10.1093/cercor/bhh092

Touboul J (2008) Bifurcation analysis of a general class of nonlinear integrate-and-fire neurons. SIAM Journal on Applied Mathematics

68(4):1045–1079
Vanier MC, Bower JM (1999) A comparative survey of automated parameter-search methods for compartmental neural models. J Comput Neurosci 7(2):149–171

Addendum: Low Threshold Spiking cells (LTS)

The preceding manuscript gives the set of parameters for three types of cortical cells. For the fourth type the LTS cell was chosen in concordance with D4-2. Experimental traces were not available for this cell type at the time of the report. The adaptive exponential model was fitted on a previous model of LTS cells (Destexhe et al. (1998)). This cell types contains a very rare ion channel, which adds important non-linear processes in the subthreshold regime. Figure A illustrates how this model reacts when a negative step current in injected. The response is asymmetric with a mono-exponential decay on the onset of the step and a large overshoot accompanied with a burst of spikes on the offset of the step current.

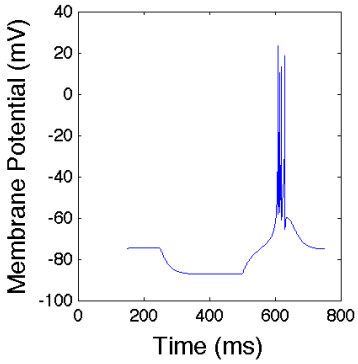

Figure A: Response of a Hodgkin and Huxley type model of LTS to a negative current step. The membrane potential makes an exponential decay on the onset of the step. The offset of the step causes a large overshoot with a burst.

The adaptive exponential is linear in a regime far from the spike initiation threshold, and there can be no linear system of equation to account for an asymmetrical response to positive or negative steps. To see this, we can write the membrane potential response as linear filter of the current $I(t) = I_0 H(t)$:

$$V(t) = \int_0^\infty \kappa(s) I(t-s) ds = I_0 \int_0^\infty \kappa(s) H(t-s) ds \equiv I_0 K(t)$$

where H(t) is zero for $t<0$ and one otherwise. The function κ can be any function. We can see that the potential response V(t) must have the same shape regardless of the sign of I_0. This reasoning shows that the adaptive exponential could not follow closely the subthreshold potential of the LTS model. The adaptive exponential can produce low threshold spikes as in the model described by: C = 140 pF, g_L = 3 nS, EL = -75 mV, V_T = -58 mV, Δ_T = 2, Er = -64 mV, a = 12 nS, b = 10 pA, τ_w = 50 ms. Figure B shows the performance of this adaptive exponential model compared with the single compartment Hodgkin and Huxley LTS model. Although a fraction of the spikes are reproduced the subthreshold voltage is not modelled with high precision.

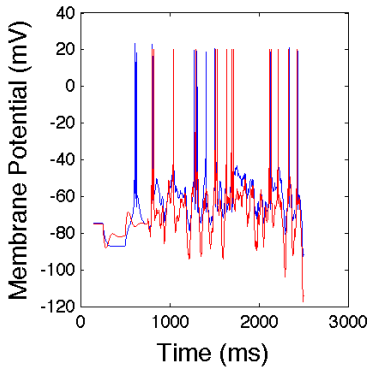

Figure B: Adaptive exponential model and LTS model from Destexhe et al. (1998) compared on the basis of noisy current injection preceded by a negative step.

Additional reference: Destexhe, A et al. J. Neurosci. (1998).